HIGH-ORDER DISCONTINUOUS GALERKIN METHODS FOR INCOMPRESSIBLE FLOWS

A. Montlaur[*], S. Fernández-Méndez[†] and A. Huerta[†]

[*] Escola Politècnica Superior de Castelldefels
[†] E.T.S. d'Enginyers de Camins, Canals i Ports de Barcelona
Laboratori de Càlcul Numèric (LaCàN), www-lacan.upc.edu
Universitat Politècnica de Catalunya
Jordi Girona 1-3, 08034 Barcelona, Spain
e-mail: {adeline.de.montlaur, sonia.fernandez, antonio.huerta}@upc.edu

Key words: Navier-Stokes equations, incompressible flow, Runge-Kutta methods, discontinuous Galerkin, solenoidal, Interior Penalty Method

Abstract. *The spatial discretization of the unsteady incompressible Navier-Stokes equations is stated as a system of Differential Algebraic Equations (DAEs), corresponding to the conservation of momentum equation plus the constraint due to the incompressibility condition. Runge-Kutta methods applied to the solution of the resulting index-2 DAE system are analyzed, allowing a critical comparison in terms of accuracy of semi-implicit and fully implicit Runge-Kutta methods. Numerical examples, considering a discontinuous Galerkin Interior Penalty Method with piecewise solenoidal approximations, demonstrate the applicability of the approach, and compare its performance with classical methods for incompressible flows.*

1 INTRODUCTION

Due to constraints of computing costs, in the past, development of numerical techniques for fluid flow simulations has focused mainly on steady state calculations. However, many physical phenomena of interest are inherently unsteady, creating the need for efficient numerical formulations for unsteady flows, a few examples being separated flows, wake flows, fluid actuators and maneuvering. Good stability properties and high orders of accuracy in time as well as in space are critical requirements, especially when studying boundary layers or high Reynolds number flows.

An important difficulty for the numerical simulation of incompressible flows is that velocity and pressure are coupled by the incompressibility constraint. Interest in using projection methods to overcome this difficulty in time-dependent viscous incompressible flows started with the introduction of fractional-step methods for the incompressible Navier-Stokes equations, see [1, 2]. Following the original ideas of Chorin and Temam, numerous authors have successfully used fractional-step methods for incompressible flows, see for instance [3, 4, 5, 6]. The pressure/incompressibility terms have to be treated implicitly while the remaining terms, viscous and convective, can be treated either explicitly, semi-implicitly or fully implicitly. Nevertheless, while explicit schemes are used at much lower cost, the number of realistic problems that are amenable to explicit formulation is very small. In common situations, large variations in element size, required to solve multiple spatial scales occurring in high Reynolds number flow or in boundary layers, make the use of explicit time integration techniques impractical. In such cases, implicit schemes have to be considered such as implicit fractional step methods, Crank-Nicolson [7], or generalized-α methods [8]. Unfortunately, these classical methods for incompressible flow are at most second-order accurate in time.

On the other hand, higher order time integrators are widely used for compressible flows, such as Backward Difference multistep methods [9] or high-order Runge-Kutta (RK) methods. In particular, it is well known that for high-order accurate computations, RK methods present two major advantages in front of multistep methods: larger stability regions and straightforward implementation of variable time step. Thus, high-order RK methods have been successfully applied to compressible flow problems, whose spatial discretization (for example with finite elements or finite volumes) leads to a system of Ordinary Differential Equations (ODEs), see [10, 11].

In this work, the possibilities of using high-order implicit RK methods for incompressible flow computations are explored. To that end, the space discretization of the unsteady incompressible Navier-Stokes equations is interpreted as an index-2 system of Differential Algebraic Equations (DAE) [12]; that is, a system of ODEs corresponding to the conservation of momentum equation, plus algebraic constraints corresponding to the incompressibility condition. This interpretation was already considered in [13] for the implementation of third and fifth-order implicit RK methods. Here a critical comparison, in terms of accuracy, of semi-implicit and fully-implicit RK methods is performed

for the solution of the unsteady Navier-Stokes equations, whereas a full stability analysis is presented in [14]. Specific RK methods are recommended for incompressible flow computations, with both unconditional stability and high-order accuracy.

Furthermore, numerical examples using a Discontinuous Galerkin (DG) formulation with solenoidal approximation allow a comparison, in terms of accuracy and computational cost, between the high-order recommended RK methods and also with other classical methods, such as the second-order Crank-Nicolson method.

The paper is structured as follows. Section 2 recalls the basic concepts of implicit RK methods for the solution of index-2 DAEs, motivated by their application to the solution of incompressible flow problems. In Section 3, the DG Interior Penalty Method proposed in [15, 16] for the steady Stokes and Navier-Stokes equations is recalled, and extended to the solution of the unsteady Navier-Stokes equations. The resulting IRK-DG scheme has high-order properties both in time and space. Moreover, the use of piecewise solenoidal approximations leads to an important reduction in the number of degrees of freedom. Numerical examples are presented in Section 4 to show the applicability of the methods, and to compare accuracy and computational cost of RK methods for index-2 DAEs with a classical Crank-Nicolson scheme.

2 DAE RUNGE-KUTTA METHODS FOR UNSTEADY INCOMPRESSIBLE FLOWS

Let $\Omega \subset \mathbb{R}^{\mathtt{n_{sd}}}$ be an open bounded domain, with boundary $\partial\Omega$, and $\mathtt{n_{sd}}$ the number of spatial dimensions. The strong form of the unsteady incompressible Navier-Stokes problem can be written as

$$\frac{\partial \boldsymbol{u}}{\partial t} - 2\boldsymbol{\nabla} \cdot (\nu\boldsymbol{\nabla}^{\mathsf{s}}\boldsymbol{u}) + \boldsymbol{\nabla}p + (\boldsymbol{u} \cdot \boldsymbol{\nabla})\boldsymbol{u} = \boldsymbol{f} \qquad \text{in } \Omega, \qquad (1a)$$

$$\boldsymbol{\nabla} \cdot \boldsymbol{u} = 0 \qquad \text{in } \Omega, \qquad (1b)$$

$$\boldsymbol{u} = \boldsymbol{u}_D \qquad \text{on } \Gamma_D, \qquad (1c)$$

$$-p\boldsymbol{n} + 2\nu(\boldsymbol{n} \cdot \boldsymbol{\nabla}^{\mathsf{s}})\boldsymbol{u} = \boldsymbol{t} \qquad \text{on } \Gamma_N, \qquad (1d)$$

where $\partial\Omega = \overline{\Gamma}_D \cup \overline{\Gamma}_N$, $\Gamma_D \cap \Gamma_N = \emptyset$, $\boldsymbol{f} \in \mathcal{L}_2(\Omega)$ is a source term, $\boldsymbol{u}$ the flux velocity, p its pressure, ν the kinematic viscosity and $\boldsymbol{\nabla}^{\mathsf{s}} = \frac{1}{2}(\boldsymbol{\nabla} + \boldsymbol{\nabla}^T)$. In (1a), the constant density has been absorbed into the pressure.

Here the space discretization of the incompressible Navier-Stokes equations is carried out using a discontinuous Galerkin Interior Penalty Method with solenoidal piecewise approximations, as detailed in Section 3. Nevertheless, the algorithms discussed in this work would be equally applicable to other types of discretization schemes, for example using other DG formulations or continuous Galerkin. In any case, the space discretization of the unsteady incompressible Navier-Stokes problem (1) can be written as

$$\begin{cases} \mathbf{M}\dot{\mathbf{u}} + \mathbf{K}\mathbf{u} + \mathbf{C}(\mathbf{u})\mathbf{u} + \mathbf{G}\mathbf{p} = \mathbf{f_1} \\ \mathbf{G}^T\mathbf{u} = \mathbf{f_2} \end{cases} \qquad (2)$$

where $\mathbf{M}$ is the mass matrix, $\mathbf{K}$ the diffusion matrix, $\mathbf{C}$ the convection matrix, $\mathbf{G}$ the pressure matrix, $\mathbf{u}$ and $\mathbf{p}$ the vectors of nodal values, or approximation coefficients of velocity and pressure respectively, and $\mathbf{f_1}$ and $\mathbf{f_2}$ vectors taking into account force term and boundary conditions, see for instance [17]. This system, of $\mathtt{n_{dof}}$ degrees of freedom, can also be written as

$$\begin{cases} \dot{\mathbf{u}} = \mathcal{F}(t, \mathbf{u}, \mathbf{p}) \\ 0 = \mathcal{G}(t, \mathbf{u}) \end{cases} \tag{3}$$

where

$$\begin{aligned} \mathcal{F}(t, \mathbf{u}, \mathbf{p}) &= \mathbf{M^{-1}} \left(\mathbf{f_1} - \mathbf{Ku} - \mathbf{C(u)u} - \mathbf{Gp} \right), \\ \mathcal{G}(t, \mathbf{u}) &= \mathbf{G}^T \mathbf{u} - \mathbf{f_2}. \end{aligned} \tag{4}$$

Note that $\frac{\partial \mathcal{G}}{\partial \mathbf{u}} \frac{\partial \mathcal{F}}{\partial \mathbf{p}} = \mathbf{G}^T \mathbf{M}^{-1} \mathbf{G}$ is invertible. Therefore, (3) is a Hessenberg index-2 DAE system [18].

DAEs originate in the modelisation of various physical or chemical phenomena and have been deeply studied during the last years [18, 19]. They are classified by their differential index, that is, the minimum number of times that a DAE system must be differentiated to obtain an ODE. For instance, the discrete incompressible Stokes, Oseen and Navier-Stokes equations are index-2 DAE systems.

Many numerical methods initially defined for ODEs have been adapted to DAEs, as for example multistep Backward Differentiation Formulae [20] or Runge-Kutta methods [19]. Runge-Kutta (RK) methods have been first regarded as poor competitors to multistep methods, mainly because for most DAEs and RK methods, the order of convergence obtained was less than the order obtained for ODEs, and the higher the index, the higher the reduction. Ulterior results from [12] have however shown that proper RK methods can form the basis of a competitive code, because they are unconditionally stable and can reach orders of convergence as high as when applied to ODE.

In this work, Runge-Kutta methods for index-2 DAE are considered [12]. An s-stage Runge-Kutta method for (3) reads

$$\begin{aligned} \mathbf{u}^{n+1} &= \mathbf{u}^n + \Delta t \sum_{i=1}^{s} b_i \mathbf{l}_i \\ \mathbf{p}^{n+1} &= \mathbf{p}^n + \Delta t \sum_{i=1}^{s} b_i \mathbf{k}_i \end{aligned} \tag{5}$$

where $\mathbf{l}_i$ and $\mathbf{k}_i$ are defined as the solution of the system

$$\mathbf{l}_i = \mathcal{F} \left(t^n + c_i \Delta t, \mathbf{u}^n + \Delta t \sum_{j=1}^{s} a_{ij} \mathbf{l}_j, \mathbf{p}^n + \Delta t \sum_{j=1}^{s} a_{ij} \mathbf{k}_j \right) \tag{6a}$$

$$0 = \mathcal{G} \left(t^n + c_i \Delta t, \mathbf{u}^n + \Delta t \sum_{j=1}^{s} a_{ij} \mathbf{l}_j \right) \tag{6b}$$

for $i = 1, ..., s$. Coefficients a_{ij}, b_i, c_i come from the Butcher array, whose general form is seen in Table 1. Depending on the specific form of the Butcher array, implicit, semi-

$$
\begin{array}{c|cccc}
c_1 & a_{11} & a_{12} & \cdots & a_{1s} \\
c_2 & a_{21} & a_{22} & \cdots & a_{2s} \\
\vdots & \vdots & \vdots & & \vdots \\
c_s & a_{s1} & a_{s2} & \cdots & a_{ss} \\
\hline
& b_1 & b_2 & \cdots & b_s
\end{array}
$$

Table 1: Butcher array

implicit or explicit Runge-Kutta methods are obtained. A Runge-Kutta method is said to be explicit if its Butcher array is strictly lower triangular, that is $a_{ij} = 0$ for $j \geq i$. Otherwise the method is implicit (IRK). In particular, an implicit method is said to be semi-implicit, or diagonally implicit (DIRK), if $a_{ij} = 0$ for $j > i$ and $a_{ii} \neq 0$ for some i. If in addition all diagonal coefficients (a_{ii}) are identical, the method is called singly diagonally implicit (SDIRK). SDIRK are of special interest for a linear problem, as for example the Stokes problem, since one may hope to use repeatedly the stored LU-factorization of the matrix. This work focuses on fully implicit and semi-implicit methods because of their stability properties. In fact, explicit Runge-Kutta methods can not even be used in the form of (5)-(6) for Hessenberg index-2 DAEs, because the resulting system (6) is under-determined to solve for $\mathbf{l}_i$ and $\mathbf{k}_i$. Nevertheless, in [21] explicit Runge-Kutta methods are applied to DAE, using a different formulation than (5)-(6). In this case, the order of convergence of explicit Runge-Kutta methods is less than the one reached for a regular ODE. For example, the 4-stage explicit RK scheme applied to the incompressible Navier-Stokes equations in [21] only leads to second-order accuracy for velocity and pressure, see [14].

2.1 IRK and SDIRK methods

Table 2 shows the order of convergence for index-2 DAE (such as the discrete incompressible Navier-Stokes problem), and for ODE, for s-stage Radau IA, IIA and Lobatto IIIC methods. Other methods, such as Gauss or Lobatto IIIA, are dismissed because they present higher order reduction when applied to DAEs with respect to ODEs. As shown in Table 2, the best orders of convergence for velocity and pressure are obtained for a Radau IIA-IRK method, keeping the order of convergence for velocity for DAEs as high as for ODEs.

Table 3 shows Butcher diagrams for 2- and 3-stage Radau IIA-IRK methods. Radau IIA-IRK methods are a special case of IRK methods satisfying the additional property $b_j = a_{sj}$ for $j = 1, \cdots, s$. These methods are called IRK(DAE) and they stand out from all IRK methods in view of their applicability to DAE since at the last stage, $\mathbf{u}^{n+1}$ directly satisfies the constraint $\mathcal{G}(t^{n+1}, \mathbf{u}^{n+1}) = 0$. Because of this additional property and of

5

Method	DAE: $\boldsymbol{u}$ error	DAE: p error	ODE error
Radau IA	h^s	h^{s-1}	h^{2s-1}
Radau IIA	h^{2s-1}	h^s	h^{2s-1}
Lobatto IIIC	h^{2s-2}	h^{s-1}	h^{2s-2}

Table 2: Orders of convergence for s-stage IRK methods for index-2 DAEs and for ODEs [22, 12].

$$
\begin{array}{c|cc}
\frac{1}{3} & \frac{5}{12} & -\frac{1}{12} \\
1 & \frac{3}{4} & \frac{1}{4} \\
\hline
 & \frac{3}{4} & \frac{1}{4}
\end{array}
\qquad
\begin{array}{c|ccc}
\frac{4-\sqrt{6}}{10} & \frac{88-7\sqrt{6}}{360} & \frac{296-169\sqrt{6}}{1800} & \frac{-2+3\sqrt{6}}{225} \\
\frac{4+\sqrt{6}}{10} & \frac{296+169\sqrt{6}}{1800} & \frac{88+7\sqrt{6}}{360} & \frac{-2-3\sqrt{6}}{225} \\
1 & \frac{16-\sqrt{6}}{36} & \frac{16+\sqrt{6}}{36} & \frac{1}{9} \\
\hline
 & \frac{16-\sqrt{6}}{36} & \frac{16+\sqrt{6}}{36} & \frac{1}{9}
\end{array}
$$

Table 3: Butcher array for 2-stage (left) and 3-stage (right) Radau IIA-IRK methods

their high orders of convergence, 2- and 3-stage Radau IIA-IRK are selected among fully-implicit RK methods to be compared from accuracy and cost points of view in Section 4.2.

Note that the solution of an index-2 DAE system, such as (3), with an s-stage fully-implicit Runge-Kutta method requires solving a non-linear system of equations of dimension $s\mathtt{n}_{\mathtt{dof}}$ at each time step, where $\mathtt{n}_{\mathtt{dof}}$ is the number of degrees of freedom in (3). An alternative to reduce the computational cost would be to use an SDIRK method.

For instance, Table 4 shows the Butcher diagram for 2-stage SDIRK method. The

$$
\begin{array}{c|cc}
\gamma & \gamma & 0 \\
1-\gamma & 1-2\gamma & \gamma \\
\hline
 & \frac{1}{2} & \frac{1}{2}
\end{array}
$$

Table 4: Butcher array for 2-stage SDIRK method, with $\gamma = \frac{3+\sqrt{3}}{6}$

computational effort in implementing semi-implicit methods is substantially less than for a fully-implicit method, indeed s systems of dimension $\mathtt{n}_{\mathtt{dof}}$ are to be solved, instead of a problem of dimension $s\mathtt{n}_{\mathtt{dof}}$ in the fully-implicit scheme.

Unfortunately, SDIRK methods do not reach high orders of convergence, as illustrated in Table 5. Unlike for ODE problems, increasing the number of stages of SDIRK methods does not improve the order of convergence for index-2 DAE systems. The order of convergence of SDIRK methods for an index-2 DAE system is limited to 2 for velocity and 1 for pressure, for 2, 3 or 5 stages [1]. Note that, this is exactly the same order as

---

[1][23] conjectured and presented some evidence for the belief that for any s even number greater than two, no SDIRK method exists with order $s + 1$ for an ODE. That is why no 4-stage method appears in Table 5.

Number of stages	DAE: $\boldsymbol{u}$ error	DAE: p error	ODE error
2	2	1	3
3	2	1	4
5	2	1	6

Table 5: Orders of convergence for SDIRK methods for index-2 DAEs and for ODEs [22, 12].

the classical Crank-Nicolson scheme, which has considerably less computational cost (one system of dimension $\mathtt{n_{dof}}$ at each time step).

Thus, in this work, fully-implicit Radau IIA-IRK methods are recommended among other RK methods for the solution of incompressible flow problems. These methods are compared in term of accuracy and computational cost with the classical Crank-Nicolson method in Section 4.2.

3 DISCONTINUOUS GALERKIN FORMULATION FOR THE UNSTEADY INCOMPRESSIBLE NAVIER-STOKES PROBLEM

The discretization of problem (1) following a DG Interior Penalty formulation [15, 16] is presented in this section. To that purpose, suppose that Ω is partitioned in $\mathtt{n_{el}}$ disjoint subdomains Ω_i,

$$\overline{\Omega} = \bigcup_{i=1}^{\mathtt{n_{el}}} \overline{\Omega}_i, \quad \Omega_i \cap \Omega_j = \emptyset \text{ for } i \neq j,$$

with piecewise linear boundaries $\partial\Omega_i$, which define an internal interphase Γ

$$\Gamma := \left[\bigcup_{i=1}^{\mathtt{n_{el}}} \partial\Omega_i \right] \backslash \partial\Omega.$$

The *jump* $[\![\cdot]\!]$ and *mean* $\{\cdot\}$ operators are defined along the interface Γ using values from the elements to the left and to the right of the interface (say, Ω_i and Ω_j) and are also extended along the exterior boundary (only values in Ω are employed), namely

$$[\![\odot]\!] = \begin{cases} \odot_i + \odot_j & \text{on } \Gamma, \\ \odot & \text{on } \partial\Omega, \end{cases} \quad \text{and} \quad \{\odot\} = \begin{cases} \kappa_i \odot_i + \kappa_j \odot_j & \text{on } \Gamma, \\ \odot & \text{on } \partial\Omega. \end{cases}$$

Usually $\kappa_i = \kappa_j = 1/2$ but, in general, these two scalars are only required to verify $\kappa_i + \kappa_j = 1$, see for instance [24]. The major difference between the mean and the jump operator is that the latter always involves the normal to the interface or to the boundary of the domain. For instance, given two contiguous subdomains Ω_i and Ω_j their exterior unit normals are denoted respectively $\boldsymbol{n}_i$ and $\boldsymbol{n}_j$ (recall that $\boldsymbol{n}_i = -\boldsymbol{n}_j$) and along $\partial\Omega$ the exterior unit normal is denoted by $\boldsymbol{n}$; the jump is then

$$[\![p\,\boldsymbol{n}]\!] = \begin{cases} p_i\,\boldsymbol{n}_i + p_j\,\boldsymbol{n}_j = \boldsymbol{n}_i(p_i - p_j) & \text{on } \Gamma \\ p\,\boldsymbol{n} & \text{on } \partial\Omega \end{cases}$$

7

for scalars, see [15] for vectors or tensors.

The following discrete finite element spaces are also introduced

$$\boldsymbol{\mathcal{V}}^h = \{\boldsymbol{v} \in [\mathcal{L}_2(\Omega)]^{\mathtt{n_{sd}}} \; ; \; \boldsymbol{v}|_{\Omega_i} \in [\mathcal{P}^k(\Omega_i)]^{\mathtt{n_{sd}}} \quad \forall \Omega_i\}$$
$$\mathcal{Q}^h = \{q \in [\mathcal{L}_2(\Omega)] \; ; \; q|_{\Omega_i} \in [\mathcal{P}^{k-1}(\Omega_i)] \quad \forall \Omega_i\}$$

where $\mathcal{P}^k(\Omega_i)$ is the space of polynomial functions of degree at most $k \geq 1$ in Ω_i.

Finally, in the following equations $(\cdot, \cdot)$ denotes the $\mathcal{L}_2$ scalar product in Ω, that is

$$(p, q) = \int_\Omega p \, q \, d\Omega \qquad\qquad \text{for scalars,}$$

$$(\boldsymbol{u}, \boldsymbol{v}) = \int_\Omega \boldsymbol{u} \cdot \boldsymbol{v} \, d\Omega \qquad\qquad \text{for vectors,}$$

$$(\boldsymbol{\sigma}, \boldsymbol{\tau}) = \int_\Omega \boldsymbol{\sigma} : \boldsymbol{\tau} \, d\Omega \qquad\qquad \text{for second-order tensors.}$$

Analogously, $(\cdot, \cdot)_\Upsilon$ denotes the $\mathcal{L}_2$ scalar product in any domain $\Upsilon \subset \Gamma \cup \partial\Omega$. For instance,

$$(p, q)_\Upsilon = \int_\Upsilon p \, q \, d\Gamma$$

for scalars.

In [16], an Interior Penalty Method was derived for the steady Navier-Stokes equations. Its extension for an unsteady formulation becomes: find $\boldsymbol{u}_h \in \boldsymbol{\mathcal{V}}^h$ and $p_h \in \mathcal{Q}^h$ such that

$$\left(\frac{\partial \boldsymbol{u}_h}{\partial t}, \boldsymbol{v}\right) + a\big(\boldsymbol{u}_h, \boldsymbol{v}\big) + c\big(\boldsymbol{u}_h; \boldsymbol{u}_h, \boldsymbol{v}\big) + b\big(\boldsymbol{v}, p_h\big) + (\{p_h\}, [\![\boldsymbol{n} \cdot \boldsymbol{v}]\!])_{\Gamma \cup \Gamma_D} = l\big(\boldsymbol{v}\big) \qquad \forall \, \boldsymbol{v} \in \boldsymbol{\mathcal{V}}^h,$$

$$b\big(\boldsymbol{u}_h, q\big) + (\{q\}, [\![\boldsymbol{n} \cdot \boldsymbol{u}_h]\!])_{\Gamma \cup \Gamma_D} = (q, \boldsymbol{n} \cdot \boldsymbol{u}_D)_{\Gamma_D} \quad \forall \, q \in \mathcal{Q}^h, \tag{7}$$

where the following forms must be defined,

$$a\big(\boldsymbol{u}, \boldsymbol{v}\big) := \big(2\nu\boldsymbol{\nabla}^{\mathbf{s}}\boldsymbol{u}, \boldsymbol{\nabla}^{\mathbf{s}}\boldsymbol{v}\big) + C_{11} \big([\![\boldsymbol{n} \otimes \boldsymbol{u}]\!], [\![\boldsymbol{n} \otimes \boldsymbol{v}]\!]\big)_{\Gamma \cup \Gamma_D}$$
$$- \big(2\nu\{\boldsymbol{\nabla}^{\mathbf{s}}\boldsymbol{u}\}, [\![\boldsymbol{n} \otimes \boldsymbol{v}]\!]\big)_{\Gamma \cup \Gamma_D} - \big([\![\boldsymbol{n} \otimes \boldsymbol{u}]\!], 2\nu\{\boldsymbol{\nabla}^{\mathbf{s}}\boldsymbol{v}\}\big)_{\Gamma \cup \Gamma_D}, \tag{8a}$$

$$l\big(\boldsymbol{v}\big) := \big(\boldsymbol{f}, \boldsymbol{v}\big) + \big(\boldsymbol{t}, \boldsymbol{v}\big)_{\Gamma_N} + C_{11} \big(\boldsymbol{u}_D, \boldsymbol{v}\big)_{\Gamma_D} - \big(\boldsymbol{n} \otimes \boldsymbol{u}_D, 2\nu\boldsymbol{\nabla}^{\mathbf{s}}\boldsymbol{v}\big)_{\Gamma_D}, \tag{8b}$$

$$c\big(\boldsymbol{w}; \boldsymbol{u}, \boldsymbol{v}\big) := \frac{1}{2}\Bigg[- \big((\boldsymbol{w} \cdot \boldsymbol{\nabla})\boldsymbol{v}, \boldsymbol{u}\big) + \big((\boldsymbol{w} \cdot \boldsymbol{\nabla})\boldsymbol{u}, \boldsymbol{v}\big) + \int_{\Gamma_N} (\boldsymbol{w} \cdot \boldsymbol{n})\boldsymbol{u} \cdot \boldsymbol{v} d\Gamma$$
$$+ \sum_{i=1}^{\mathtt{n_{el}}} \int_{\partial\Omega_i \backslash \Gamma_N} \frac{1}{2} \big[(\boldsymbol{w} \cdot \boldsymbol{n}_i)(\boldsymbol{u}^{ext} + \boldsymbol{u}) - |\boldsymbol{w} \cdot \boldsymbol{n}_i| (\boldsymbol{u}^{ext} - \boldsymbol{u})\big] \cdot \boldsymbol{v} d\Gamma\Bigg] \tag{9a}$$

and

$$b(\boldsymbol{v}, p) := - \int_\Omega q \, \boldsymbol{\nabla} \cdot \boldsymbol{v} \, d\Omega, \tag{9b}$$

The penalty parameter, a positive scalar C_{11} of order $\mathcal{O}(h^{-1})$, must be large enough to ensure coercivity of the bilinear form $a(\cdot, \cdot)$, see [15]. The characteristic mesh size is denoted by h. A standard upwind numerical flux, see for instance [25], is used for the definition of the convective term $c(\cdot; \cdot, \cdot)$. In (9a), $\boldsymbol{u}^{ext}$ denotes the exterior trace of $\boldsymbol{u}$ taken over the side/face under consideration, that is

$$\boldsymbol{u}^{ext}(\boldsymbol{x}) = \lim_{\varepsilon \to 0^+} \boldsymbol{u}(\boldsymbol{x} + \varepsilon \boldsymbol{n}_i) \qquad \text{for } \boldsymbol{x} \in \partial \Omega_i.$$

Remark 1 *Possible alternatives to the IPM formulation proposed here are for example the Local Discontinous Galerkin (LDG) method [26, 27], and the Compact Discontinous Galerkin (CDG) method [28]. In [16], IPM and CDG methods are compared for the solution of the Navier-Stokes equations, concluding that both methods present similar results for the accuracy of the numerical solution, reaching optimal convergence rates for velocity and pressure. The main differences are that CDG is less sensitive to the selection of the penalty parameter, but has the major disadvantage of the implementation and computation of lifting operators.*

Remark 2 *Note that in [16] the convective term was defined as*

$$c(\boldsymbol{w}; \boldsymbol{u}, \boldsymbol{v}) := -((\boldsymbol{w} \cdot \boldsymbol{\nabla})\boldsymbol{v}, \boldsymbol{u}) + \int_{\Gamma_N} (\boldsymbol{w} \cdot \boldsymbol{n}) \boldsymbol{u} \cdot \boldsymbol{v} d\Gamma$$
$$+ \sum_{i=1}^{n_{el}} \int_{\partial \Omega_i \backslash \Gamma_N} \frac{1}{2} \left[(\boldsymbol{w} \cdot \boldsymbol{n}_i)(\boldsymbol{u}^{ext} + \boldsymbol{u}) - |\boldsymbol{w} \cdot \boldsymbol{n}_i| (\boldsymbol{u}^{ext} - \boldsymbol{u}) \right] \cdot \boldsymbol{v} d\Gamma. \tag{10}$$

Nevertheless, when solving the unsteady incompressible Navier-Stokes equations, the original convective term of the strong form, $(\boldsymbol{u} \cdot \boldsymbol{\nabla})\boldsymbol{u}$ can be replaced by $(\boldsymbol{u} \cdot \boldsymbol{\nabla})\boldsymbol{u} - \frac{1}{2}(\boldsymbol{\nabla} \cdot \boldsymbol{u})\boldsymbol{u}$, which is a legitimate modification for a divergence-free velocity field [2]. This guarantees unconditional stability, in the case of an implicit or semi-implicit time integration [17]. The trilinear convective term defined in (9a) is skew-symmetric, that is, $c(\boldsymbol{w}; \boldsymbol{u}, \boldsymbol{u}) = 0$.

Following [26, 15, 27], the velocity space $\boldsymbol{\mathcal{V}}^h$ is now split into direct sum of a solenoidal part and an irrotational part $\boldsymbol{\mathcal{V}}^h = \boldsymbol{\mathcal{S}}^h \oplus \boldsymbol{\mathcal{I}}^h$, where

$$\boldsymbol{\mathcal{S}}^h = \left\{ \boldsymbol{v} \in [\mathcal{H}^1(\Omega)]^{n_{sd}} \mid \boldsymbol{v}|_{\Omega_i} \in [\mathcal{P}^k(\Omega_i)]^{n_{sd}}, \, \boldsymbol{\nabla} \cdot \boldsymbol{v}|_{\Omega_i} = 0 \text{ for } i = 1, \ldots, n_{el} \right\},$$
$$\boldsymbol{\mathcal{I}}^h \subset \left\{ \boldsymbol{v} \in [\mathcal{H}^1(\Omega)]^{n_{sd}} \mid \boldsymbol{v}|_{\Omega_i} \in [\mathcal{P}^k(\Omega_i)]^{n_{sd}}, \, \boldsymbol{\nabla} \times \boldsymbol{v}|_{\Omega_i} = \boldsymbol{0} \text{ for } i = 1, \ldots, n_{el} \right\}.$$

For instance, a solenoidal basis in a 2D triangle for an approximation of degree $k = 2$ is

$$\boldsymbol{\mathcal{S}}^h = \left\langle \begin{pmatrix} 1 \\ 0 \end{pmatrix}, \begin{pmatrix} 0 \\ 1 \end{pmatrix}, \begin{pmatrix} 0 \\ x \end{pmatrix}, \begin{pmatrix} x \\ -y \end{pmatrix}, \begin{pmatrix} y \\ 0 \end{pmatrix}, \begin{pmatrix} 0 \\ x^2 \end{pmatrix}, \begin{pmatrix} 2xy \\ -y^2 \end{pmatrix}, \begin{pmatrix} x^2 \\ -2xy \end{pmatrix}, \begin{pmatrix} y^2 \\ 0 \end{pmatrix} \right\rangle,$$

and the irrotational complementary part for $k = 2$ is

$$\boldsymbol{\mathcal{I}}^h = \left\langle \begin{pmatrix} x \\ 0 \end{pmatrix}, \begin{pmatrix} x^2 \\ 0 \end{pmatrix}, \begin{pmatrix} 0 \\ y^2 \end{pmatrix} \right\rangle,$$

see for example [29] for the construction of these spaces.

Under these circumstances, IPM problem (7) can be split in two *uncoupled* problems. The first one solves for *divergence-free* velocities and *hybrid pressures*: find $\boldsymbol{u}_h \in \boldsymbol{\mathcal{S}}^h$ and $\tilde{p}_h \in \boldsymbol{P}^h$ solution of

$$
\begin{cases}
\left(\dfrac{\partial \boldsymbol{u}_h}{\partial t}, \boldsymbol{v} \right) + a\left(\boldsymbol{u}_h, \boldsymbol{v}\right) + c\left(\boldsymbol{u}_h; \boldsymbol{u}_h, \boldsymbol{v}\right) + (\tilde{p}_h, [\![\boldsymbol{n} \cdot \boldsymbol{v}]\!])_{\Gamma \cup \Gamma_D} = l\left(\boldsymbol{v}\right) & \forall \boldsymbol{v} \in \boldsymbol{\mathcal{S}}^h, \\[2mm]
(\tilde{q}, [\![\boldsymbol{n} \cdot \boldsymbol{u}_h]\!])_{\Gamma \cup \Gamma_D} = (\tilde{q}, \boldsymbol{n} \cdot \boldsymbol{u}_D)_{\Gamma_D} & \forall \tilde{q} \in \boldsymbol{P}^h,
\end{cases}
$$

(11)

with the forms defined in (8), (9b) and (9a). Note that this problem, which has to be solved at each time step, shows an important reduction in the number of degrees of freedom with respect to problem (7), as explained in [16].

The space of hybrid pressures (pressures along the sides in 2D or faces in 3D) is simply:

$$\boldsymbol{P}^h := \left\{ \tilde{p} \mid \tilde{p} : \Gamma \cup \Gamma_D \longrightarrow \mathbb{R} \text{ and } \tilde{p} = [\![\boldsymbol{n} \cdot \boldsymbol{v}]\!] \text{ for some } \boldsymbol{v} \in \boldsymbol{\mathcal{S}}^h \right\}.$$

In fact, reference [26] demonstrates that $\boldsymbol{P}^h$ corresponds to piecewise polynomial pressures in the element sides in 2D or faces in 3D.

The second problem, which requires the solution of the previous one, evaluates *interior* pressures: find $p_h \in \mathcal{Q}^h$ such that

$$b\left(\boldsymbol{v}, p_h\right) = l\left(\boldsymbol{v}\right) - \left(\frac{\partial \boldsymbol{u}_h}{\partial t}, \boldsymbol{v} \right) - a\left(\boldsymbol{u}_h, \boldsymbol{v}\right) - (\tilde{p}_h, [\![\boldsymbol{n} \cdot \boldsymbol{v}]\!])_{\Gamma \cup \Gamma_D} - c\left(\boldsymbol{u}_h; \boldsymbol{u}_h, \boldsymbol{v}\right) \quad \forall \boldsymbol{v} \in \boldsymbol{\mathcal{I}}^h. \quad (12)$$

It is important to note that equation (12) can be solved element by element and pressure is its only unknown. The second problem (12) is a postprocess that allows to compute pressure in the elements' interior, usually at the end of the computation, or after the iterations in each time step. For example, if interior pressure p_h needs to be calculated at time t^n, (12) is solved at t^n, where $\boldsymbol{u}_h^t$ can be approximated using

$$\left. \frac{\partial \boldsymbol{u}_h}{\partial t} \right|^n = \frac{\boldsymbol{u}_h^{t^n} - \boldsymbol{u}_h^{t^{n-1}}}{\Delta t}, \text{ for first-order accuracy in time,} \tag{13a}$$

$$\left. \frac{\partial \boldsymbol{u}_h}{\partial t} \right|^n = \frac{\boldsymbol{u}_h^{t^{n+1}} - \boldsymbol{u}_h^{t^{n-1}}}{2\Delta t}, \text{ for second-order accuracy in time,} \tag{13b}$$

$$\left. \frac{\partial \boldsymbol{u}_h}{\partial t} \right|^n = \frac{-\boldsymbol{u}_h^{t^{n+2}} + 8\boldsymbol{u}_h^{t^{n+1}} - 8\boldsymbol{u}_h^{t^{n-1}} + \boldsymbol{u}_h^{t^{n-2}}}{12\Delta t}, \text{ for fourth-order accuracy in time.} \tag{13c}$$

To preserve the high order of convergence of hybrid pressure obtained with Radau IIA-IRK methods, formulation (13c) is the most suitable for interior pressure recovery.

4 NUMERICAL EXAMPLES

Numerical examples are now considered to show the applicability of the proposed methods. First, the flow past a circle example is used to show the good behavior of the proposed methods. An example with analytical solution is then used to compare RK methods with a classical Crank Nicolson method from accuracy and cost points of view. In both examples, the discontinuous Galerkin IPM formulation with piecewise solenoidal approximations described in Section 3 is used.

4.1 Flow past a circle

In the present section we consider a mixed Dirichlet/Neumann problem simulating the flow past a circle, with diameter $D = 1$, in a uniform stream. In this example, a high-order mesh generator *EZ4U* is used, see [30].

An unstructured mesh of 472 fourth-order elements is used, as seen in Figure 1. These fourth-order elements are used for numerical integration and post-process. Fourth-order piecewise solenoidal approximation for the velocity is also used ($k = 4$) and third-order for pressure, see Section 3. Dirichlet boundary condition $\boldsymbol{u}_D = (1, 0)$ is imposed on the inlet

(a) Mesh of the total domain   (b) Zoom in the vicinity of the circle
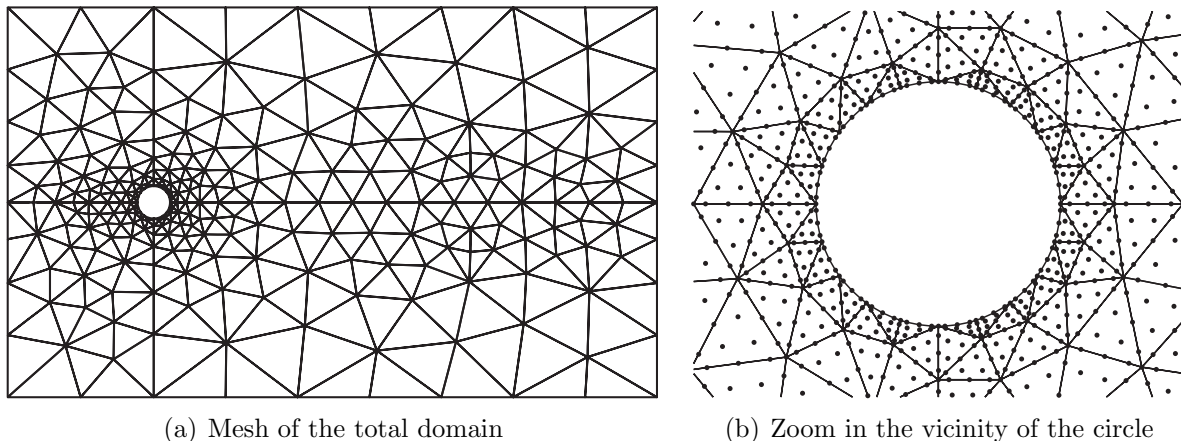
Figure 1: Flow past a circle: unstructured mesh of 472 fourth-order elements

and no-slip condition, $\boldsymbol{u}_D = (0, 0)$, on the circle. Null Neumann conditions are imposed on the three other sides. Initial conditions prescribe a unitary velocity field $\boldsymbol{u}_0 = (1, 0)$ on the whole domain, except on the circle boundary where $\boldsymbol{u}_0 = (0, 0)$. 3-stage Radau IIA-IRK is used for time integration. The flow pattern depends on the Reynolds number defined here as $Re = \frac{u_\infty D}{\nu}$, where u_∞ is the mean fluid velocity, here $u_\infty = 1$.

For low Reynolds number ($1 \leq Re \leq 50$), it is well known that the solution reaches a stationary state. Here a Reynolds number of $Re = 100$ is considered, leading to an unsteady solution. A time step $\Delta t = 0.03$ is used on the time interval $[0, 100]$, and $\Delta t = 0.005$ on $[100, 120]$, to better capture the period of the periodic flow pattern. Once

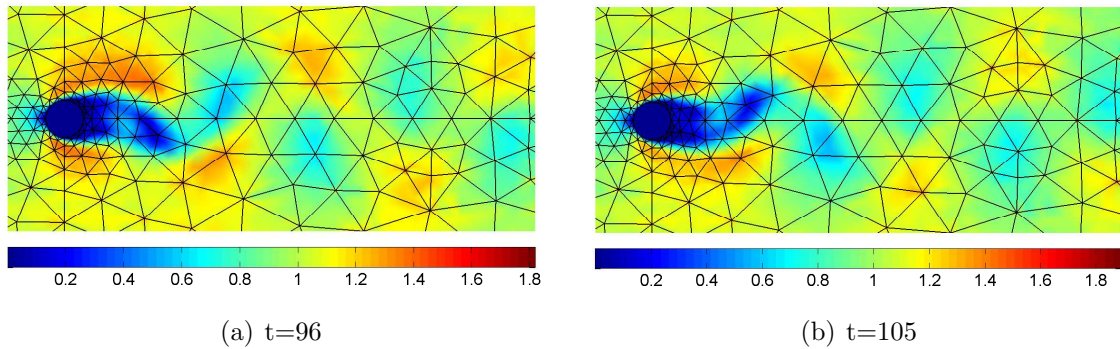(a) t=96   (b) t=105

Figure 2: Flow past a circle: velocity module of the flow for $Re = 100$, periodic phase.

the flow passes the transient phase and reaches a periodic solution, vortex shedding is observed, that is, the flow detaches successively from the top and from the bottom of the sphere creating vortices behind the circle as seen in Figure 2 and more precisely in Figure 3. This happens in an alternating fashion and this non-symmetric flow pattern is known as Von Karman vortex.

(a) t=96   (b) t=105
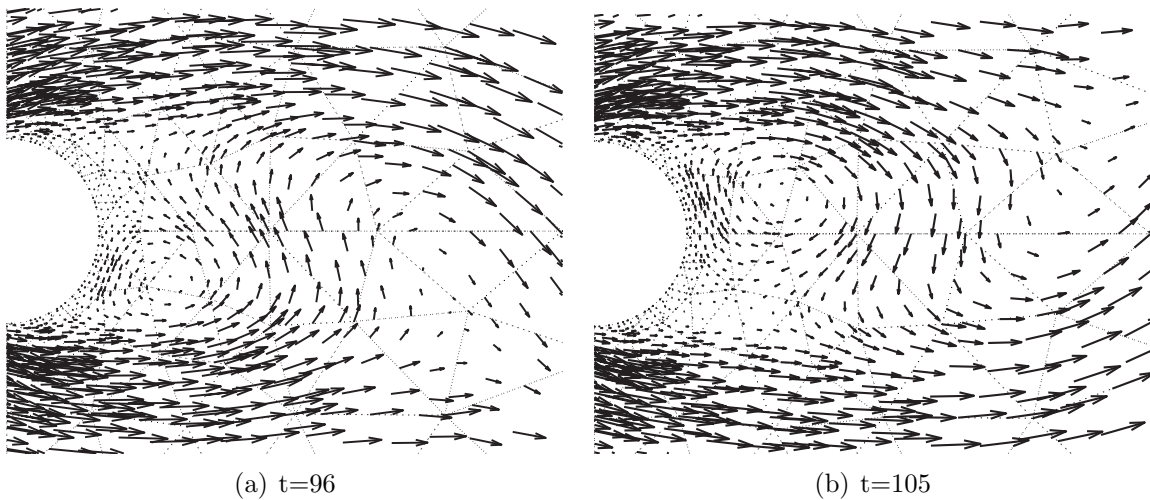
Figure 3: Flow past a circle: velocity vectors in the vicinity of the circle for $Re = 100$, periodic phase.

The periodic behavior of the solution is also captured by the evolution of the lift coefficient C_L, which is defined by the following integral along the circle

$$C_L = \int_0^{2\pi} \boldsymbol{\tau}_y d\boldsymbol{\theta}$$

where $\boldsymbol{\tau}_y$ is the y-component of the normal component of the Cauchy stress tensor $\boldsymbol{\tau} = -p\boldsymbol{n} + 2\nu(\boldsymbol{n} \cdot \boldsymbol{\nabla}^{\mathsf{s}})\boldsymbol{u}$. Figure 4 shows C_L as a function of time. After a transient phase, the flow pattern reaches the periodic solution, showing the frequency of the Von Karman
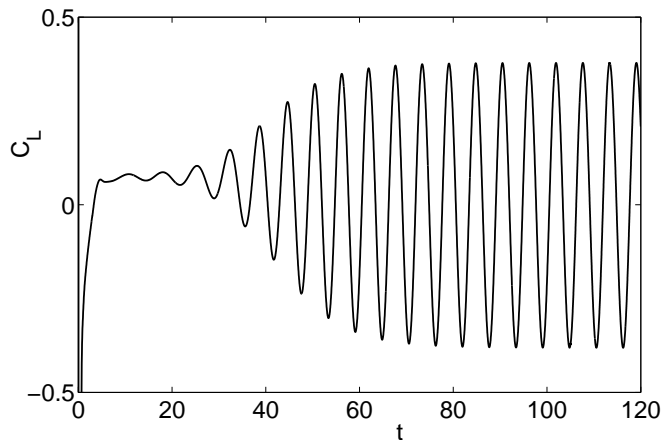
12

Figure 4: Flow past a circle: evolution of the lift coefficient with time

vortex. Roshko, see [31], experimentally established the relation between the Strouhal number and the Reynolds number, for flows past a circle and for Reynolds numbers between 90 and 150 as

$$S = 0.212 \left(1 - \frac{21.2}{Re} \right). \tag{14}$$

The Strouhal number is a dimensionless number describing oscillating flow mechanisms, defined from the frequency of vortex shedding f_S as

$$S = \frac{f_S D}{u_\infty},$$

with D and u_∞ characteristic lengths and velocity of the problem previously defined. In Figure 4, the period of the periodic movement is measured and is found equal to $T = 5.96$, which corresponds to $S = 0.1678$, which is in good agreement with experimental results and reported numerical simulations from [31] and [32], as seen in Table 6. Note that in

	3-stage IRK	2-stage IRK	Roshko (14)	Simo [32]
S	0.168	0.168	0.1671	0.167

Table 6: Flow past a circle: Strouhal number results for $Re = 100$

order to obtain a better measure of the period T, the time step Δt has been set up to a value of 0.005 on a few periods, once the periodic solution is reached. The same value of Strouhal number is obtained when using a 2-stage IRK method, confirming the general good performance of the Radau IIA-IRK methods, for the solution of the incompressible Navier-Stokes problem.

4.2 Runge-Kutta and Crank-Nicolson accuracy and cost comparison

An example with analytical solution proposed in [5] is used to compare the accuracy and cost of 2- and 3- stage Radau IIA-IRK and Crank-Nicolson (CN) methods, which are all unconditionally stable methods for incompressible Navier-Stokes problems.

The incompressible Navier-Stokes equations are solved in a 2D square domain $\Omega =]0, \frac{1}{2}[\times]0, \frac{1}{2}[$ with Dirichlet boundary conditions on three sides and Neumann boundary condition on the fourth side $\{x = 0\}$. A body force

$$\boldsymbol{f} = \begin{pmatrix} 2\nu sin(x+t)sin(y+t) + cos(x-y+t) + sin(x+y+2t) + sin(x+t)cos(x+t) \\ 2\nu cos(x+t)cos(y+t) - cos(x-y+t) - sin(x+y+2t) - sin(y+t)cos(y+t) \end{pmatrix}$$

is imposed in order to have the exact solution

$$\boldsymbol{u} = \begin{pmatrix} sin(x+t)sin(y+t) \\ cos(x+t)cos(y+t) \end{pmatrix},$$

$$p = sin(x-y+t),$$

Polynomial interpolation of degree $k = 4$ for velocity and 3 for pressure is chosen and an unstructured mesh of 128 elements is used, with $0.01 \le h \le 0.1$. The calculation is made until a final time $t = 40$. Initial condition prescribes exact solution on the whole domain.
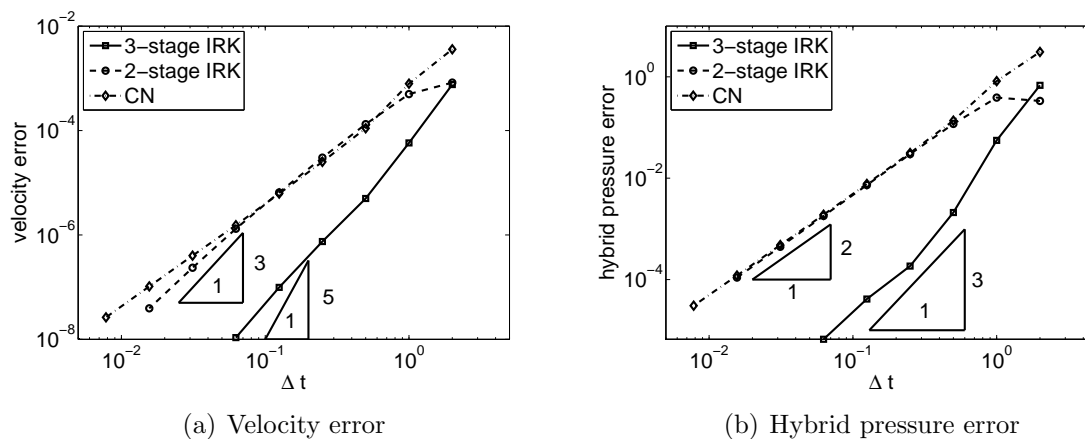

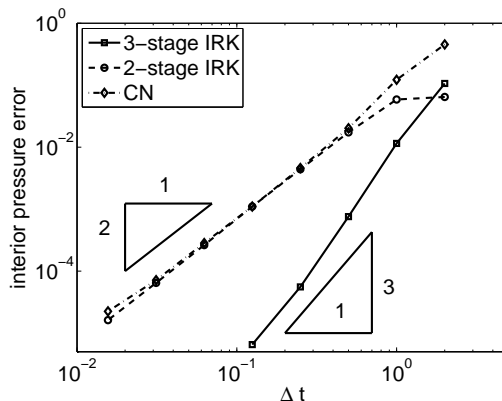(a) Velocity error   (b) Hybrid pressure error

Figure 5: Unsteady analytical example: velocity and hybrid pressure $\mathcal{L}_2$-errors for 3-stage and 2-stage IRK and CN methods, $k = 4$, $0.01 \le h \le 0.1$.

Figure 5 shows the evolution of the $\mathcal{L}_2$-error under Δt-refinement when solving (11) for velocity and hybrid pressure. CN exhibits its theoretical convergence rate, 2 for both velocity and pressure, whereas IRK methods present optimal convergence rates for hybrid

14

pressure, respectively 2 and 3 for 2- and 3-stage IRK methods, but suboptimal convergence rates for velocity: almost 4 instead of 5 for the 3-stage IRK scheme, and around 2.6 instead of 3 for the 2-stage IRK scheme. Nevertheless, it is worth noticing the increasing slope of the convergence curves. This behavior has also been observed in scalar toy numerical tests, showing almost optimal convergence rates for smaller time steps. In any case, as expected from the theoretical orders of convergence, for the same time step clearly higher accuracy and convergence rate is obtained with the 3-stage IRK method.

Figure 6: Unsteady analytical example: interior pressure $\mathcal{L}_2$-errors for 3-stage and 2-stage IRK and CN methods, $k = 4$, $0.01 \leq h \leq 0.1$.

Figure 6 shows the evolution of the $\mathcal{L}_2$-error of the interior pressure, obtained as a post-process, solving (12) with the time derivative fourth-order approximation (13c). For all methods, interior pressure reaches optimal order of convergence.

Figures 5 and 6 show how, for the same time step, the high-order 3-stage IRK method provides higher accuracy compared to the classical CN method or to the 2-stage IRK method. Nevertheless, it is also the most expensive method. Compared to CN, the 3-stage IRK method requires three times more evaluations of the convective residue, and leads to a three-time larger linear system of equations to be solved at each iteration. Thus, is it necessary to see if its higher accuracy balances its high computational cost.

A comparison of accuracy in terms of computational cost is presented in the following, but let us first recall that one of the main motivations of using high-order time integrators is to achieve similar accuracy in time and space. For instance, for fourth-order space discretization, the global error is expected to behave as

$$e = c_1 h^4 + c_2 \Delta t^r$$

where r is the order of the time integrator. Assuming that a characteristic mesh size is $h = 0.1$, the order of magnitude of precision obtained in space is around 10^{-4}. If a scheme like 3-stage Radau IIA-IRK, reaching fourth or fifth order in time, is used, a time step of

15

$\Delta t = 0.1$ can be considered to reach equivalent accuracy in time and in space. Whereas if a second-order method as for example CN, is used, a time step of $\Delta t = 0.01$ has to be taken. This means that ten times more time steps are needed with CN than with 3-stage Radau IIA-IRK to reach the same time accuracy. Note that Figure 5(a) confirms this fact, the velocity error obtained with 3-stage Radau IIA-IRK for a time step of $\Delta t = 0.1$ is equivalent to the one obtained with a CN scheme for $\Delta t \approx 0.01$.

Now let us compare the cost of both methods. As previously commented, 3-stage Radau IIA-IRK requires three evaluations of the convective residue when only one evaluation is needed for CN. At each iteration, it has been checked for 3-stage Radau IIA-IRK that almost 90% of the CPU time is spent in evaluating the convective residue and only 10% in other operations such as the solution of linear systems. Thus, roughly speaking, 3-stage Radau IIA-IRK is three times more expensive than CN at each iteration. In both cases a Broyden method is used to solve the non-linear system and the same number of iterations is needed to solve the non-linear system at each time step. Since 3-stage Radau IIA-IRK needs about ten times less time steps than CN to reach equivalent precision for velocity, globally and for high levels of precision, 3-stage Radau IIA-IRK is three times more efficient than CN. The same comparison can be made with hybrid pressure. Though the differences are not that obvious because levels of precision for pressure are more similar, 3-stage IRK is again more efficient than CN. The following study confirms these numbers.

Figure 7 compares the $\mathcal{L}_2$-errors of velocity and hybrid pressures obtained with 2- and 3- stage Radau IIA-IRK and Crank-Nicolson methods as a function of CPU cost needed. For low accuracy, all methods have an equivalent precision-to-cost ratio both for velocity
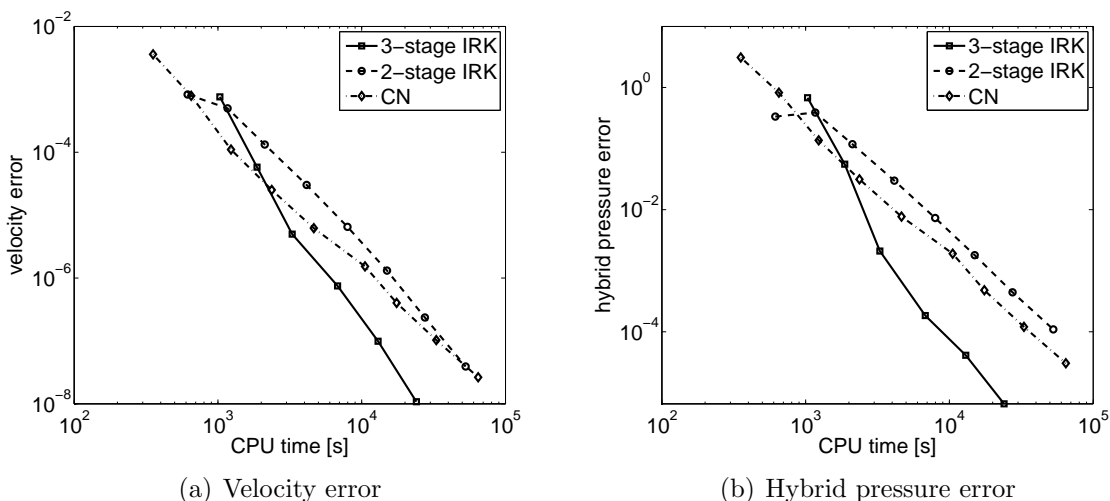

(a) Velocity error   (b) Hybrid pressure error

Figure 7: Unsteady analytical example: velocity and hybrid pressure $\mathcal{L}_2$-errors, as a function of CPU cost for 3-stage and 2-stage IRK and CN methods, $k = 4$, $0.01 \leq h \leq 0.1$.

and hybrid pressures and the CN method seems to be the best option. But when higher

accuracy is wanted, that is for example for an error less than 10^{-4} for velocity and less than 10^{-2} for hybrid pressure, the higher order of convergence of 3-stage Radau IIA-IRK balances its higher cost per iteration, and it becomes the most efficient method. Figure 8 shows the $\mathcal{L}_2$-error of interior pressure, obtained from (12) using a fourth-order
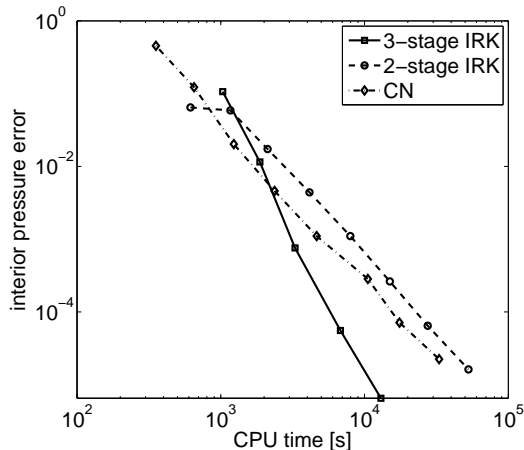

Figure 8: Unsteady analytical example: interior pressure $\mathcal{L}_2$-error, as a function of CPU cost for 3-stage and 2-stage IRK and CN methods, $k = 4$, $0.01 \leq h \leq 0.1$.

approximation for the time derivative, as a function of CPU cost. Again 3-stage Radau IIA-IRK is the most efficient scheme when high accuracy is required. Note that this example shows that 3-stage Radau IIA-IRK method is promising but more complex and $3D$ examples will have to be considered to confirm this trend.

5 CONCLUSIONS

- Semi-implicit (SDIRK) and fully-implicit Runge-Kutta (IRK) methods are considered to solve the unsteady incompressible Navier-Stokes equations, stated as a system of Differential Algebraic Equations, but IRK are eventually preferred since they reach higher order of time accuracy.

- Between the available IRK schemes, Radau IIA-IRK methods are chosen because, for a given number of stages, they reach the highest order of convergence, with the same order of convergence for velocity as for ODEs.

- For 2D classical examples, the resulting IRK time integration scheme is very competitive, compared to a classical Crank Nicolson method, and is more efficient when high accuracy is required.

- A high-order discontinuous Galerkin Interior Penalty Method, with solenoidal approximations, is used for space discretization, allowing to reach high orders of accuracy in space as well as in time.

17

REFERENCES

[1] A. Chorin, "Numerical solution of the Navier-Stokes equations," *Math. Comp.*, vol. 22, no. 104, pp. 745–762, 1968.

[2] R. Temam, *Navier-Stokes equations - Theory and numerical analysis*. AMS Chelsea Publishing, 2001.

[3] J. Donea, S. Giuliani, H. Laval, and L. Quartapelle, "Finite element solution of the unsteady Navier-Stokes equations by a fractional step method," *Comput. Meth. Appl. Mech. Eng.*, vol. 30, pp. 53–73, 1981.

[4] J. Kim and P. Moin, "Application of a fractional-step method to incompressible Navier-Stokes equations," *J. Comput. Phys.*, vol. 59, pp. 308–323, 1985.

[5] J. Guermond, P. Minev, and J. Shen, "An overview of projection methods for incompressible flows," *Comput. Meth. Appl. Mech. Eng.*, vol. 195, pp. 6011–6045, 2006.

[6] M. Houzeaux, M. Vázquez, and R. Aubry, "A massively parallel fractional step solver for incompressible flows," *J. Comput. Phys.*, no. Accepted for publication, 2009.

[7] K. Kim, S.-J. Baek, and H. Jin Sung, "An implicit velocity decoupling procedure for the incompressible Navier-Stokes equations," *Int. J. Numer. Methods Fluids*, vol. 38, no. 2, pp. 125–138, 2002.

[8] K. Jansen, C. Whiting, and G. Hulbert, "A generalized-α method for integrating the filtered Navier-Stokes equations with a stabilized finite element method," *Comput. Meth. Appl. Mech. Eng.*, vol. 190, no. 3, pp. 305–319, 2000.

[9] P.-O. Persson and J. Peraire, "Newton-GMRES preconditioning for discontinuous Galerkin discretizations of the Navier-Stokes equations," *SIAM J. Sci. Comput.*, vol. 30, no. 6, pp. 2709–2733, 2008.

[10] F. Bassi and S. Rebay, "A high-order accurate discontinuous finite element method for the numerical solution of the compressible Navier-Stokes equations," *J. Comput. Phys.*, vol. 131, no. 2, pp. 267–279, 1997.

[11] L. Wang and D. J. Mavriplis, "Implicit solution of the unsteady Euler equations for high-order accurate discontinuous Galerkin discretizations," *J. Comput. Phys.*, vol. 225, no. 2, pp. 1994–2015, 2007.

[12] E. Hairer and G. Wanner, *Solving Ordinary Differential Equations II- Stiff and Differential-Algebraic Problems*. Springer-Verlag, 1991.

[13] S. Étienne, A. Garon, and D. Pelletier, "Perspective on the geometric conservation law and finite element methods for ALE simulations of incompressible flow," *J. Comput. Phys.*, vol. 228, pp. 2313–2333, 2009.

[14] A. Montlaur, *High-order discontinuous Galerkin methods for incompressible flows.* PhD thesis, Universitat Politènica de Catalunya, 2009. http://www.tesisenxarxa.net/TDX-0122110-183128.

[15] A. Montlaur, S. Fernandez-Mendez, and A. Huerta, "Discontinuous Galerkin methods for the Stokes equations using divergence-free approximations," *Int. J. Numer. Methods Fluids*, vol. 57, no. 9, pp. 1071–1092, 2008.

[16] A. Montlaur, S. Fernandez-Mendez, J. Peraire, and A. Huerta, "Discontinuous Galerkin methods for the Navier-Stokes equations using solenoidal approximations," *Int. J. Numer. Methods Fluids*, no. Accepted for publication, 2009.

[17] J. Donea and A. Huerta, *Finite element methods for flow problems.* Chichester: John Wiley & Sons, 2003.

[18] E. Hairer, C. Lubich, and M. Roche, *The Numerical Solution of Differential-Algebraic Systems by Runge-Kutta Methods.* Springer-Verlag, 1989.

[19] K. Brenan, S. Campbell, and L. Petzold, *Numerical Solution of Initial-Value Problems in Differential-Algebraic Equations.* SIAM, 1996.

[20] K. E. Brenan and B. E. Engquist, "Backward differentiation approximations of nonlinear differential/algebraic systems," *Math. Comp.*, vol. 51, no. 184, pp. 659–676, 1988.

[21] J. M. C. Pereira, M. Kobayashi, and J. C. F. Pereira, "A fourth-order-accurate finite volume compact method for the incompressible Navier-Stokes solutions," *J. Comput. Phys.*, vol. 167, no. 1, pp. 217–243, 2001.

[22] J. Butcher, *The numerical analysis of ordinary differential equations.* Wiley, 1987.

[23] S. Norsett, "One-step methods of hermite type for numerical integration of stiff systems," *BIT*, vol. 14, pp. 63–77, 1974.

[24] A. Hansbo and P. Hansbo, "A finite element method for the simulation of strong and weak discontinuities in solid mechanics," *Comput. Meth. Appl. Mech. Eng.*, vol. 193, no. 33-35, pp. 3523–3540, 2004.

[25] G. Kanschat and D. Schötzau, "Energy norm a posteriori error estimation for divergence-free discontinuous Galerkin approximations of the Navier-Stokes equations," *Int. J. Numer. Methods Fluids*, vol. 57, no. 9, pp. 1093 – 1113, 2008.

[26] B. Cockburn and J. Gopalakrishnan, "Incompressible finite elements via hybridization. Part I: the Stokes system in two space dimensions," *SIAM J. Numer. Anal.*, vol. 43, no. 4, pp. 1627–1650, 2005.

[27] J. Carrero, B. Cockburn, and D. Schötzau, "Hybridized globally divergence-free LDG methods. Part I: The Stokes problem," *Math. Comp.*, vol. 75, no. 254, pp. 533–563, 2005.

[28] J. Peraire and P.-O. Persson, "The Compact Discontinuous Galerkin (CDG) method for elliptic problems," *SIAM J. Sci. Stat. Comput.*, vol. 30, no. 4, pp. 1806–1824, 2008.

[29] G. A. Baker, W. N. Jureidini, and O. A. Karakashian, "Piecewise solenoidal vector fields and the Stokes problem," *SIAM J. Numer. Anal.*, vol. 27, no. 6, pp. 1466–1485, 1990.

[30] X. Roca, J. Sarrate, and E. Ruiz-Gironès, "A graphical modeling and mesh generation environment for simulations based on boundary representation data," in *Congresso de Métodos Numéricos em Engenharia, Porto, Portugal, 2007*, 2007.

[31] A. Roshko, "On the development of turbulent wakes from vortex streets," *NACA Report*, no. 1191, 1954.

[32] J. Simo and F. Armero, "Unconditional stability and long-term behaviour of transient algorithms for the incompressible Navier Stokes and Euler equations," *Comput. Meth. Appl. Mech. Eng.*, vol. 111, pp. 111–154, 1994.